

Feedback and Environmental Effects in Elliptical Galaxies

Craig L. Sarazin

Abstract The role of the environment of an elliptical galaxy on its hot interstellar gas is discussed. In general, the X-ray halos of early-type galaxies tend to be smaller and fainter in denser environments, with the exception of group-central galaxies. X-ray observations show many examples of nearby galaxies which are undergoing gas stripping. On the other hand, most bright galaxies in clusters do manage to retain small coronae of X-ray emission. Recent theoretical and observational results on the role of feedback from AGN at the centers of elliptical galaxies on their interstellar gas are reviewed. X-ray observations show many examples of X-ray holes in the central regions of brightest-cluster galaxies; in many cases, the X-ray holes are filled with radio lobes. Similar radio bubbles are seen in groups and individual early-type galaxies. “Ghost bubbles” are often seen at larger radii in clusters and galaxies; these bubbles are faint in high radio frequencies, and are believed to be old radio bubbles which have risen buoyantly in the hot gas. Low frequency radio observations show that many of the ghost bubbles have radio emission; in general, these long wavelength observations show that radio sources are much larger and involve greater energies than had been previously thought. The radio bubbles can be used to estimate the total energy output of the radio jets. The total energies deposited by radio jets exceed the losses from the gas due to radiative cooling, indicating that radio sources are energetically capable of heating the cooling core gas and preventing rapid cooling.

1 Introduction

In this chapter, I will review some aspects of the interaction of the hot gas in elliptical galaxies with other physical elements in or around the galaxies. First, the

Craig L. Sarazin
Department of Astronomy, University of Virginia, P.O. Box 400325, Charlottesville, VA 22904-4325, USA, e-mail: sarazin@virginia.edu

interaction of the hot gas with external aspects of the environment of the elliptical will be discussed. I will concentrate on the question of whether the X-ray luminosity and gas mass of the hot interstellar medium (ISM) in ellipticals is affected by the environment. Is there more or less hot gas and X-ray emission associated with ellipticals in dense as compared to sparse environments? I will also review some of the evidence that gas in ellipticals is stripped by ram pressure due to motions through the external intergalactic gas.

The second major topic is the interaction of the hot gas in ellipticals with the active galactic nuclei (AGNs) often located at their centers. I will describe X-ray and radio evidence for this interactions, and discuss whether the AGNs can heat the X-ray gas and keep it from cooling rapidly. I will discuss evidence for feedback linking the activity by the center supermassive black hole (SMBH) and the heating and cooling of the X-ray gas. I will include both brightest cluster galaxies (BCGs) at the centers of cool core clusters of galaxies, and non-central giant ellipticals. In addition to a general review, I will present some more recent results on sound waves and shocks generated by the radio sources in the BCG in Abell 2052, the extended system of X-ray cavities and tunnels and low frequency radio emission in the BCG in Abell 262, and the southwest radio lobe in Centaurus A, the nearest bright elliptical and nearest radio galaxy.

2 Environmental Effects on X-ray Emission

2.1 X-ray Luminosity vs. Density

Given the wide range in X-ray luminosities of early-type galaxies of a given optical luminosity, the question naturally arises as to whether part of this dispersion might be due to the effects of environment on their X-ray emission. In particular, are galaxies in dense environments more or less X-ray luminous than galaxies in sparse environments?

One difficulty is deciding what observational probe to use to assess the local density. The best choice physically depends on the mechanism for changing the X-ray luminosity one wishes to consider (e.g., tidal stripping, ram pressure stripping, etc.) Ideally, one should do the comparison for a number of different density measures. Unfortunately, it is difficult to determine the intergalactic gas density in sparse regions. As a result, the galaxy density is often used as a proxy for the density of all forms of matter. In most cases, there is insufficient data to reconstruct the three dimensional galaxy distribution, and the projected galaxy density is used instead. Of course, the fact that a galaxy is projected against a region of high galaxy projected density is no guarantee that it is actually located in a high density region.

Another complication arises from the fact that current hot gas content of an early-type galaxy probably depends on its history, rather than only on its current location.

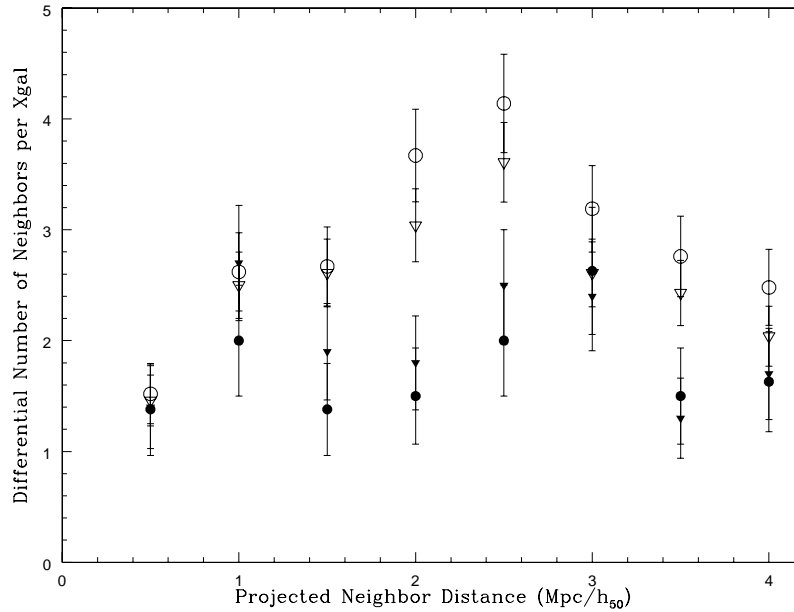


Fig. 1 Distribution of the number of bright galaxy neighbors around galaxies with X-ray detections or limits as a function of the projected distance from the X-ray galaxy. This figure is adapted from White and Sarazin [1, Fig. 13]. The filled circles (triangles) are for galaxies with higher than average X-ray luminosities (triangles include upper limits). The open circles and triangles are for usually faint X-ray galaxies.

At the expected stellar mass loss rates, it may require a long time to replenish gas which was removed in the past.

Another issue is separating the X-ray emission from an individual galaxy from that due to the surrounding group or cluster. The higher spatial resolution of Chandra and XMM-Newton observations have helped to separate galaxy and group emission. However, in earlier observations of group-central early-type galaxies, the group emission was often included in the flux of the galaxy. Also, group-central galaxies are often brighter than other optically similar galaxies, and studies have reached very different conclusions depending on whether such galaxies are included or not.

Finally, if one is interested in the hot gas content of elliptical galaxies, one must remove the contribution from a central AGN or X-ray binaries and other stellar sources. The high resolution of Chandra observations has been particularly useful for this.

White and Sarazin [1] suggested that elliptical galaxies in dense environments were fainter than those in sparse regions. Fig. 1 illustrates their result, which indicated that X-ray luminous early-type galaxies had fewer neighboring bright galaxies in projection. Their work was based on Einstein observations of early-type galaxies.

The local density was characterized by the projected galaxy density in the region around the target galaxy. They suggested that this correlation was due to ram pressure stripping of gas from galaxies (see Sect. 2.3 below).

A study of pairs of galaxies based on ROSAT data also found that the galaxies were generally underluminous compared to isolated galaxies [2]. It is unlikely that this is due to ram pressure stripping, but it might be due to tidal effects. A recent Chandra study of galaxies in groups also found an anti-correlation of local density and emission [3].

An XMM-Newton study of galaxies in the Coma cluster found that, on average, they were 5.6 times less luminous than similar galaxies in lower density locations [4]; this result was confirmed by a smaller Chandra study of Coma [5]. In general, Chandra studies of galaxies in clusters [e.g., 6, 7] also seem to confirm a general anti-correlation of local density and X-ray luminosity. In these dense and complex regions, a reduction in the gas mass might be due to ram pressure stripping, viscous or evaporative stripping, gravitational effects, mergers, or some other mechanism.

Alternatively, using ROSAT data Brown and Bregman [8] argued that early-type galaxies in dense regions were more luminous. They suggested that the hot galactic gas in denser groups was confined by the pressure of intergalactic gas. Their sample included a number of group-central ellipticals; in these systems, it can be uncertain as to what fraction of the emission is due to galactic or group gas.

A number of other studies of the relation between X-ray luminosity and local density based on ROSAT data found no correlation [e.g., 9, 10, 11]. Helsdon et al. [10] studied galaxies in groups. They separated group and galaxy emission. Group-central early-type galaxies were highly overluminous, and they argued that some of the earlier correlations were driven by the inclusion of these galaxies or of group X-ray emission. They found a significant scatter of X-ray luminosities for a fixed optical luminosity, but no variation with local density.

Recently, Mulchaey and Jeltama [12] found that the X-ray—optical relationship was steeper for field early-type galaxies than group or cluster galaxies. They suggested that optically faint galaxies in low density environments have their hot gas removed by winds driven by either supernovae or AGNs, and that these outflows are suppressed in regions with denser intergalactic gas. On the other hand, they argued that some galaxies in dense environments have their gas removed by ram pressure stripping, and that this occurs for both massive and low mass galaxies.

At the other end of the range of galactic environments, Memola et al. [13] studied of four very isolated elliptical galaxies with Chandra, XMM-Newton, and/or ASCA. They found that these galaxies showed a very wide range of X-ray-to-optical luminosity ratios, suggesting that environment alone cannot account for all of the dispersion in the X-ray properties of ellipticals. They suggest that age may play an important role.

2.2 *Temperature Gradients vs. Environment*

Diehl and Statler [14] found that the temperature gradient in the outer parts of elliptical galaxies correlated positively with the projected density of galaxies. Galaxies in dense regions had positive gradients, while galaxies in sparse regions had negative temperature gradients. This might be due to intergalactic gas, which might confine the galactic gas, or add to it by inflow, or heat it by thermal conduction.

2.3 *Ram Pressure Stripping of Hot Gas from Early-Type Galaxies*

The environments of elliptical galaxies tend to be denser regions than average, and in many cases have significant amounts of intergalactic gas. This is particularly true in clusters of galaxies. Clusters and groups have significant dark matter halos, which give large masses and deep gravitational potential wells. Thus, most of the galaxies in clusters and rich groups move rather rapidly through the cluster the intergalactic gas, either as a result of their individual orbits or the motions of merging subclusters. The rapid motions through the intracluster gas imply that a large ram pressure from the intergalactic gas will act on the interstellar gas of these galaxies, and may strip the gas [15]. Gunn and Gott considered the stripping of gaseous disks from galaxies, and much of the subsequent work was considered the stripping of disks. However, for ellipticals it is more interesting to consider the stripping of spherical or ellipsoidal halos of hot gas. Then, an approximate condition for stripping in a spherical galaxy is that the ram pressure satisfy

$$P_{\text{ram}} \equiv \rho_{\text{IGM}} v^2 \gtrsim 2 \frac{GM_{\text{gal}}(r)\rho_{\text{ISM}}(r)}{r}, \quad (1)$$

where ρ_{IGM} and ρ_{ISM} are the mass density of the intergalactic gas and galaxy gas halo, respectively, v is relative velocity of the galaxy and intergalactic gas, M_{gal} is the mass of the galaxy, and r is the radius from the center of the galaxy [16, 17]. Acreman et al. [18] made a series of simulations of ram pressure stripping of spherical galaxies falling into clusters of galaxies. In addition to ram pressure tails, their simulation showed contact discontinuities (“cold fronts”) at the leading edges of the galaxies. Recently, McCarty et al. [17] calculated an extensive grid of hydrodynamic simulations of the ram pressure stripping of spherical hot gas halos from galaxies due to ram pressure. They found that a parameterized version of Eq. 1 when combined with a simple parameterized expression for the time scale for stripping reproduced the simulations quite well. Other numerical simulations have confirmed this basic conclusion [e.g., 19, 20], although most of the simulations have been done for spiral galaxies.

Gas stripping can be affected and increased by related transport processes in clusters of galaxies. Viscosity and turbulence may affect the stripping of gas from early-type galaxies [21]. Nulsen found that the time scale for laminar viscous strip-

ping and stripping due to turbulence is given roughly by

$$t_{\text{vs}} \approx \frac{4R}{3v} \left(\frac{\rho_{\text{ISM}}}{\rho_{\text{IGM}}} \right) \left(\frac{12}{\text{Re}} + 1 \right)^{-1}, \quad (2)$$

where R is the radius of the galaxy, and Re is the Reynolds number of the flow. This can be faster than ram pressure stripping. However, one caution is that the viscous stresses may saturate, since the mean free paths of ions are similar to the sizes of galaxies. Moreover, both viscosity and turbulence may be reduced by the magnetic field.

For early-type galaxies in hot clusters of galaxies, thermal evaporation due to heat conduction may also help to strip any interstellar gas. If one ignores the temperature of the hot interstellar gas, the galaxy gravitational potential, cooling, and full Spitzer [22] conduction, the rate of stripping is given approximately by [23]

$$\dot{M}_{\text{ev}} \approx \frac{16\pi\mu m_p \kappa R}{25k} \approx 700 \left(\frac{T_{\text{ICM}}}{10^8 \text{ K}} \right)^{5/2} \left(\frac{R}{20 \text{ kpc}} \right) \left(\frac{\ln \Lambda}{40} \right)^{-1} M_{\odot} \text{ yr}^{-1}, \quad (3)$$

where μm_p is the mean mass per particle, T is the temperature of the intracluster gas, κ is the thermal conductivity, and $\ln \Lambda$ is the Coulomb logarithm [22]. The evaporation rate will be significantly reduced if the conductivity saturates, as is probably the case at least for disk galaxies. Unfortunately, thermal conductivity also depends critically on the magnetic field geometry. If the conductivity is not suppressed by the magnetic field, this mechanism can play an important role in stripping gas from galaxies.

There is a simple connection between mass loss by evaporation and mass loss by laminar viscosity (the Re term in Eq. 2), as pointed out by Nulsen [21]. At low velocities, the viscous term dominates, and the viscous stripping rate is nearly independent of velocity, because the Reynolds number is proportional to velocity. Since both thermal conduction and ionic viscosity are transport processes and the ion and electron mean free paths are essentially equal, the rates of stripping from these two processes are simply related:

$$\dot{M}_{\text{ev}} \approx 3.5 \dot{M}_{\text{vs}}. \quad (4)$$

This expression assumes full Spitzer thermal conduction and viscosity [22].

Brüggen and De Lucia [24] used the results from the Millennium Simulation of large scale structure to determine the ram pressure histories of galaxies in clusters. They found that $\gtrsim 64\%$ of the galaxies in clusters today should have experienced strong ram pressures ($> 10^{-11} \text{ dyn cm}^{-2}$) and thus should have undergone strong gas loss.

The innsbruck group [e.g., 25] has made very detailed simulations of the stripping of galaxies in clusters and the effect this has on the abundances of the intracluster medium (ICM). They argue that ram pressure stripping accounts for $\sim 10\%$ of the metals in the ICM, and that stripping should produce complex patterns of stripes and plumes in abundance maps of clusters.

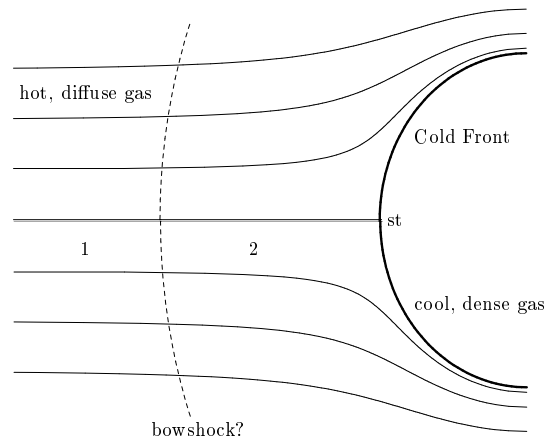


Fig. 2 A schematic diagram of flow around a “cold front”. The heavy solid arc at the right represents the contact discontinuity between the cold, dense galactic gas, and the hotter, more diffuse intergalactic gas. The galaxy is moving toward the left relative to the hotter gas. The narrow solid lines are streamlines of the flow of the hotter gas around the cold core. The region labelled “1” represent the upstream, undisturbed hot gas. If the cold front is moving transonically (Mach number $\mathcal{M} > 1$), then the cold front will be preceded by a bow shock, which is shown as a dashed arc. The stagnation point, where the relative velocity of the cooler dense gas and hotter diffuse gas is zero, is marked “st”.

2.3.1 Features Due to Ram Pressure Stripping

There are several characteristic features in X-ray images of elliptical galaxies which are expected as a result of ram pressure stripping. First, one expects a tail of hot gas behind the galaxy if the galaxies motion has a significant component in the plane of the sky. Typically, the gas from within the galaxy will be cooler and have higher metallicities than the intergalactic gas through which the galaxy is moving. Thus, the tail will be cooler and more metal-rich than the nearby intergalactic gas. Since the gas in the tail will tend to be close to pressure equilibrium with the surrounding gas, the density in the cool ram pressure tails will be higher than that of the intergalactic gas. Thus, the tails are expected to be regions of enhanced X-ray surface brightness.

Unless instabilities lead to rapid mixing of the galactic and intergalactic gas, one would expect a sharp contact discontinuity at the front of the galaxy in the direction of its relative motion. This contact discontinuity separates galactic and intergalactic gas. Again, the galactic gas will generally be cooler and more metal-rich, so this contact discontinuity will separate cooler and more metal-rich gas (the inner galactic gas) from hotter, lower abundance gas (the outer intergalactic gas). For this reason, these contact discontinuities are called “cold fronts” [26]. A schematic diagram of a cold front is shown in Fig. 2. The discontinuities associated with ram pressure stripping of galaxies are the analogs of the cold fronts associated with subclusters

in merging clusters of galaxies [26, 27]. For a very comprehensive review of this subject, see Markevitch and Vikhlinin [28].

Because cold fronts are contact discontinuities rather than shocks, the pressure varies continuously across the center of the cold front. This means that the cooler inner gas will be much denser than the hotter intergalactic gas. Since the X-ray emissivity of a gas depends on the square of its density, this implies that cold fronts will be very strong discontinuities in X-ray surface brightness. Thus, these features tend to be very noticeable in X-ray images.

As discussed extensively in [26, 28], the variation in the density, pressure, and temperature of the gas in a cold front can be used to determine the relative velocity of cool core. The geometry is illustrated in Fig. 2, which is drawn in the rest frame of the cool core. We assume that the cool core has a smoothly curved, blunt front edge. The normal component of the flow of hot gas past the surface of the cool core will be zero. There will be at least one point where the flow is perpendicular to the surface of the cool core, and the flow velocity of the hot gas will be zero at this stagnation point (“st” in Fig. 2). Far upstream, the flow of the hot gas will be undisturbed at the velocity of the cool core relative to the hotter gas, v_1 . Let c_{s1} be the sound speed in this upstream gas, and $\mathcal{M} \equiv v_1/c_{s1}$ be the Mach number of the motion of the cool core into the upstream gas. If $\mathcal{M} > 1$, a bow shock will be located ahead of the cold front.

The ratio of the pressure at the stagnation point to that far upstream is given by [e.g., 29, Sect. 114]

$$\frac{P_{\text{st}}}{P_1} = \begin{cases} \left(1 + \frac{\gamma-1}{2} \mathcal{M}^2\right)^{\frac{\gamma}{\gamma-1}}, & \mathcal{M} \leq 1, \\ \mathcal{M}^2 \left(\frac{\gamma+1}{2}\right)^{\frac{\gamma+1}{\gamma-1}} \left(\gamma - \frac{\gamma-1}{2} \mathcal{M}^2\right)^{-\frac{1}{\gamma-1}}, & \mathcal{M} > 1. \end{cases} \quad (5)$$

Here, $\gamma = 5/3$ is the adiabatic index of the gas. The ratio (P_{st}/P_1) increases continuously and monotonically with \mathcal{M} . Thus, in principle, measurements of P_1 and P_{st} in the hot gas could be used to determine \mathcal{M} . The pressures would be determined from X-ray spectra and images. In practice, the emissivity of the hot gas near the stagnation point is likely to be small. However, the pressure is continuous across the cold front, so the stagnation pressure can be determined just inside of the cool core, where the X-ray emissivity is likely to be much higher. Once \mathcal{M} has been determined, the velocity of the encounter is given by $v_1 = \mathcal{M} c_{s1}$.

If the motion of the cold front is transonic ($\mathcal{M} > 1$), one would also expect to see a bow shock front ahead of the cold front. This would be a second surface brightness discontinuity in the X-ray image. Unlike a cold front, in a bow shock the gas density, temperature, pressure, and entropy would all increase. Unfortunately, bow shock fronts are much less prominent in X-ray images than cold fronts.

The variation in the hydrodynamical properties across a bow shock are determined by the standard Rankine–Hugoniot jump conditions [e.g., 29, Sect. 85]. Let the subscripts 1 and 2 denote the preshock and postshock gas; thus, $v_1 = v_s$ is the longitudinal velocity of material into the shock (or alternative, the speed with which the shock is advancing into the preshock gas). The jump conditions can be rewritten

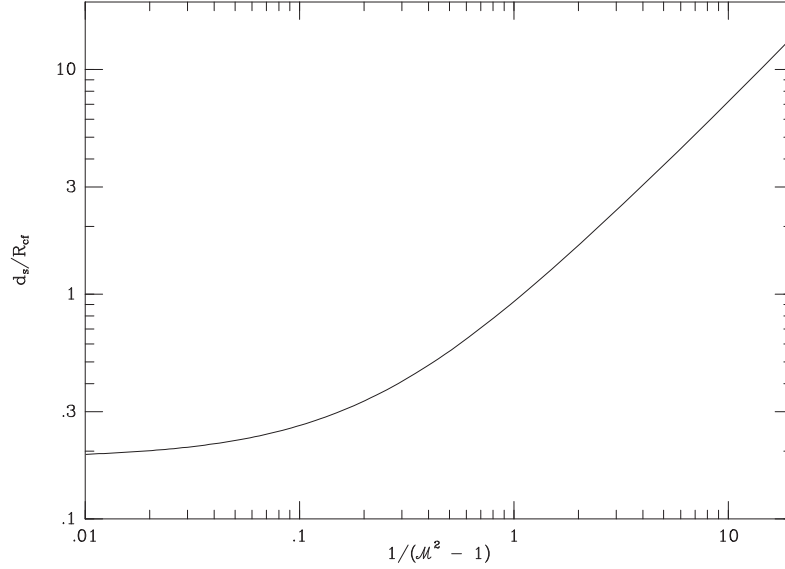


Fig. 3 The ratio of the stand-off distance of the bow shock d_s to the radius of curvature R_{cf} of the stagnation region of the cold front, as a function of $1/(\mathcal{M}^2 - 1)$, where \mathcal{M} is the Mach number. This is for a spherical cold front and $\gamma = 5/3$.

as:

$$\frac{P_2}{P_1} = \frac{2\gamma}{\gamma+1} \mathcal{M}^2 - \frac{\gamma-1}{\gamma+1}$$

$$\frac{v_2}{v_1} = \frac{\rho_1}{\rho_2} \equiv \frac{1}{C} = \frac{2}{\gamma+1} \frac{1}{\mathcal{M}^2} + \frac{\gamma-1}{\gamma+1}, \quad (6)$$

where P is the gas pressure, ρ is the gas density, v is the velocity, and $C \equiv \rho_2/\rho_1$ is the shock compression. These expressions can be used to determine the Mach number and speed of a galaxy relative to the intergalactic medium.

If the bow shock can be traced to a large transverse distance and forms a cone, the opening angle of this Mach cone corresponds to the Mach angle, $\theta_M \equiv \csc^{-1}(\mathcal{M})$. This expression could also be used to determine the galaxy Mach number [30]. However, variations in the cluster gas temperature may lead to distortions in this shape.

The bow shock will be located at some distance ahead of the cold front. The distance between the stagnation point and the closest point on the bow shock (the shock “stand-off” distance d_s) can also be used to estimate the Mach number of the motion of the cold front [26, 28]. The ratio of d_s to the radius of curvature of the cold front R_{cf} depends on the Mach number \mathcal{M} and on the shape of the cold front. Fig. 3 shows the values of d_s/R_{cf} as a function of $(\mathcal{M}^2 - 1)^{-1}$ for a spherical cold

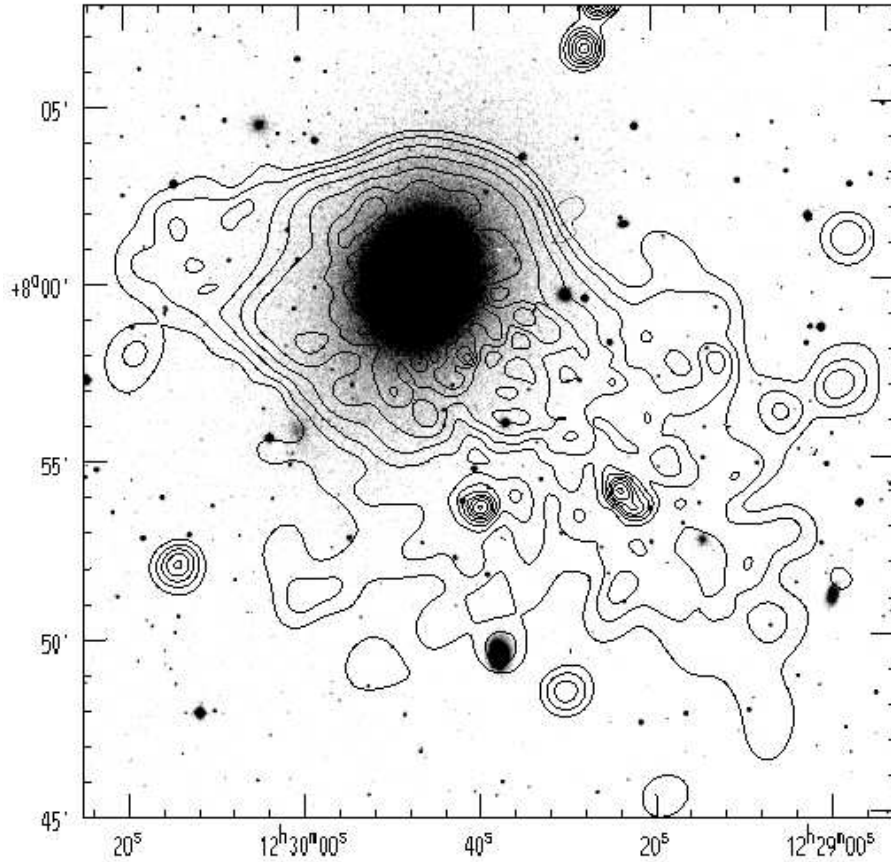


Fig. 4 Contours show the ROSAT PSPC+HRI image of the bright elliptical galaxy NGC 4472, adapted from [32]. The grey-scale is the optical image. Note the bow-shock/contact discontinuity feature to the north, and the ram pressure tail to the southwest.

front [31]. The stand-off distance increases as the Mach number approaches unity; thus, this method is, in some ways, a very sensitive diagnostic for the Mach number for the low values which often occur with galaxies in groups or clusters.

2.3.2 Examples of Ram Pressure Stripping

Observations of several elliptical galaxies in nearby clusters show evidence for ram pressure stripping.

One of the most prominent X-ray tails associated with ram pressure stripping occurs in the Virgo cluster galaxy NGC 4406 (M86) [33, 34, 35]. It shows a plume to the north, which breaks up into two tails. The total projected length of the plume and tails is 150 kpc. Based on the velocities in the systems, Randall et al. [35]

suggest that the true length is likely to be at least 380 kpc. The total mass of hot gas in the plume and tails exceeds that with the galaxy by a factor of ~ 3 , indicating that most of the gas from the galaxy is being stripped. Randall et al. [35] suggest that the position of the plume and the double tails are due to the asymmetric gravitational potential of this galaxy.

The galaxy NGC 4472 (M49) is probably the most luminous galaxy in the Virgo cluster. It is at the center of a group which appears to be falling into the cluster from the south. It shows an extended tail to the southwest, which is probably due to ram pressure [32, 36, 37]. Fig. 4 show the ROSAT X-ray image of NGC 4472 [32]. The tail extends at least 36 kpc in projection, and probably at least 100 kpc in three dimensions. There is a sharp bow-shaped surface brightness discontinuity (a cold front) ~ 21 kpc to the north of the galaxy [32, 36, 37]; XMM-Newton spectra indicate that this feature is a contact discontinuity between the interstellar gas of NGC 4472 and the Virgo intracluster gas [37]. The corresponding bow shock is not seen. Another unusual feature is that the cold front (to the north) is not 180° from the tail (to the southwest). Which of these two features represents the true direction of infall of NGC 4472 into the Virgo clusters? Irwin and Sarazin [32] suggested that NGC 4472 is moving to the north (the direction suggested by the cold front) and that the direction of the tail is affected by the ellipsoidal potential of the galaxy. Alternatively, Kraft et al. [37] recently argued that NGC 4472 is moving to the northeast as suggested by the direction of the tail, and that location and shape of the cold front are affected by more complex dynamics and by gas motions behind the cold front.

Another Virgo elliptical, NGC 4552 (M89), also shows a ram pressure tail of hot gas [38]. It has a cold front as well. It appears to be moving rather rapidly relative to the Virgo cluster gas ($v \approx 1680 \text{ km s}^{-1}$, Mach number $\mathcal{M} \approx 2.2$).

NGC 7619 in the Pegasus I group has a long X-ray tail, indicating that it is undergoing ram pressure stripping [39, 40]. The high iron abundance in the tail indicates that it came from the galaxy, rather than being a galactic wake, for example. On the opposite side of the galaxy from the tail, there is a discontinuity in the X-ray surface brightness [40, 41], which may be associated with a jump in temperature as well. This feature is consistent with a slightly supersonic shock (Mach number ~ 1), indicating that the galaxy is moving at $\sim 500 \text{ km s}^{-1}$ relative to the intergalactic gas. NGC 7619 is one of two dominant galaxies in the group; the other, NGC 7676, has a cold front which is antiparallel to that of NGC 7619. This suggests that the motions producing the ram pressure on NGC 7619 are due to a merger of two subgroups centered on these two galaxies [41].

Some other galaxies with possible ram pressure tails include NGC 1404 in the Fornax cluster [42, 43], NGC 1265 in the Perseus cluster [44], NGC 1603 in the NGC 1600 group [45], NGC 4783 in the NGC 4782 group [46], 4C34.16 [47], and C153 in the Abell 2125 cluster [48].

2.3.3 Cluster Ellipticals Retain Small Coronae

Despite the efficiency of stripping, most bright early-type galaxies in clusters do retain small coronae [7, 49]. Vikhlinin et al. [49] found that the two D galaxies near the center of the Coma cluster each retain a small corona with a temperature of 1–2 keV, a radius of ~ 3 kpc, and a gas mass of $\sim 10^8 M_{\odot}$. They suggested that the coronae were maintained by a balance between radiative cooling and highly attenuated thermal conduction.

NGC 3309 and NGC 3311, two giant elliptical galaxies near the center of the Abell 1060 cluster have small coronae similar to those in Coma [50]. The gas at the outer edge of these coronae is in pressure equilibrium with the intracluster gas.

Sun et al. [51] detected small coronae around 4 early-type galaxies in the northwest subcluster of Abell 1367. The two larger ellipticals (NGC 3837 and NGC 3842) had larger symmetrical coronae while the two less optically luminous galaxies (NGC 3841 and CGCG 97090) had smaller, disturbed, asymmetric coronae. This indicates that larger galaxies are better able to retain their gas in clusters. Comparisons with other clusters suggested that the coronae get smaller and fainter in X-rays as the ICM pressure increases.

Sun et al. [7] surveyed 157 early-type galaxies in 25 hot clusters. Most had small coronae; this was true of $>60\%$ of galaxies brighter than L^* , the characteristic luminosity of galaxies. The coronae around ellipticals in hot clusters are generally smaller (~ 2 kpc in radius), cooler (temperatures ~ 1 keV), less luminous in X-rays, and have smaller gas masses ($\sim 10^7 M_{\odot}$) than the halos around galaxies in sparser environments, indicating that most of the gas has been stripped. However, these ellipticals do retain coronae against the effects of ram pressure, thermal conduction, and input from AGN outbursts (Sect. 3 below). Remarkably, these coronae are smaller than the mean-free-path of particles in the ICM, indicating that magnetic fields must retard diffusion. To avoid being evaporated, thermal conduction must be suppressed by at least two orders of magnitude compared to the Spitzer value [22]. The cooling times of the gas in these small but dense coronae are short, making these systems miniature versions of cluster cool cores around brightest cluster galaxies. The short cooling time implies that the gas would cool quickly; its presence in many cluster ellipticals indicates that there is a heat source to maintain the gas.

X-ray coronae with short cooling times are a common feature of radio AGNs associated with group or cluster galaxies [52]. When these galaxies are the brightest cluster galaxies (BCGs) at the centers of clusters, the gas forms a cool core in the cluster. When these galaxies are not located in the centers of clusters, the cool cores are the small coronae associated with individual ellipticals.

3 AGN Feedback in Early-Type Galaxies

In recent years, evidence has been found for a coupling between supermassive black holes (SMBHs) in the centers of galaxies, and their galaxy hosts. First, the masses

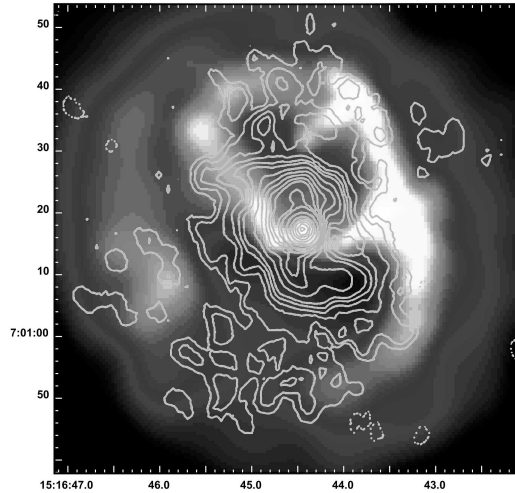


Fig. 5 Greyscale is the Chandra X-ray image of the BCG in the cool core cluster Abell 2052, showing holes in the X-ray emission surrounded by bright rims [53, 54]. The contours are the radio emission, which fills the X-ray holes. This figure is adapted from [53].

of the SMBHs are proportional to the bulge mass of the host, suggesting that star formation and SMBH accretion are connected, and that stellar bulges and SMBHs grow together [e.g., 55, 56]. Second, the optical/IR luminosity function of galaxies falls below that expected for dark matter halos at high masses in a way that can be understood if AGN suppress star formation in massive galaxies [e.g., 57].

Finally, less gas cools to low temperatures at the centers of cool core clusters, groups, and individual ellipticals than expected unless something heats the gas, and AGNs are the leading candidates [see 58, 59, for reviews]. In cool core clusters, the central cooling time is less than $\sim 7 \times 10^9$ years, and often is as short as $\sim 10^8$ years [e.g., 60]. These cool core clusters have positive temperature gradients in their centers, which are consistent with the ICM cooling down to $\sim 1/3$ of its initial temperature. Yet, the spectra indicate that $\lesssim 5\%$ of this gas continues to cool down to low temperatures [e.g., 58]. Although there are several other possibilities, the leading candidate for the required heat source is energy input from the central SMBH. In fact, the BCGs at the centers of cool core clusters are, in almost every known case, radio galaxies.

3.1 Radio Bubbles in BCGs in Clusters

Chandra and XMM-Newton observations have provided dramatic evidence for the interaction of these radio sources with the intracluster gas. In cool core clusters,

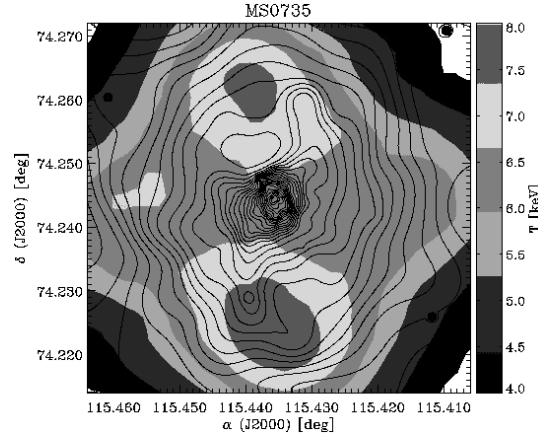


Fig. 6 Greyscale is the Chandra temperature map of the center of the cluster MS0735.6+7421, while the contours are the X-ray surface brightness, adapted from [66]. The radio bubbles in this cluster are bounded by hot regions, which indicates that the radio source is driving shocks into the intracluster gas.

X-ray deficits (“radio bubbles”) have been found at the locations of the lobes of the radio sources associated with the brightest cluster galaxies [e.g., 53, 61]. Fig. 5 shows the central region of the BCG in the Abell 2052 cluster in X-rays and radio [53, 54]. In the X-ray, these radio bubbles generally show two holes in the X-ray surface brightness on opposite sides of the galaxy nucleus. In most cases, the holes are surrounded by bright shells of X-ray emission. The X-ray holes correspond to the lobes of the central radio source. For the systems with a relatively simple geometry, deprojection analysis indicates that the X-ray surface brightness in the holes is consistent with foreground and background cluster emission; that is, the holes appear to be empty of X-ray emitting gas. The masses of X-ray gas in the surrounding shells are consistent with the mass which is missing from the holes [54]. All of this is in accord with a picture in which the central radio source has sent out two jets, which have been stopped in the cooling core gas. The jets have inflated two lobes, and the radio plasma has displaced the X-ray gas and compressed it into the two surrounding shells. In a few cases, similar radio bubbles were seen originally with ROSAT [62, 63, 64, 65]. The most spectacular case, in terms of the details in the observations, is the Perseus cluster, where there is a very long Chandra total exposure [61]. The properties of radio bubbles are reviewed in [59].

X-ray spectral observations show that the X-ray bright shells around radio bubbles are generally cool, and that the pressures in these shells are similar to those of the surrounding hotter gas. This indicates that these shells are not due to shocks, and that the radio sources are not expanding very supersonically. However, a few clusters have been found in which the radio lobes are surrounded by shells of hot gas, indicating that the radio sources are driving moderately strong shocks. Examples

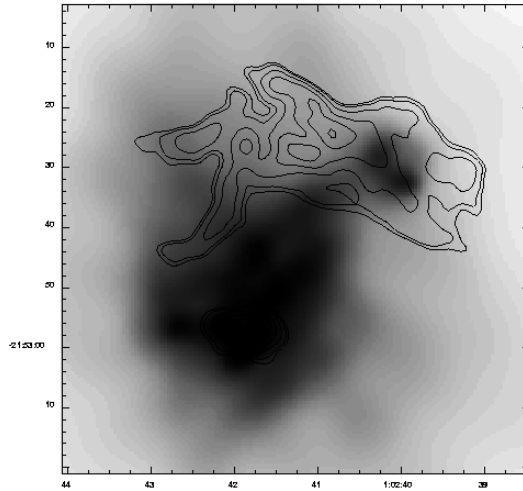


Fig. 7 Chandra X-ray image (greyscale) of the center of Abell 133, with radio contours superposed. This figure is adapted from [71]. There is a column of cool, dense, X-ray bright gas extending from the nucleus (at the lower left) to the extended radio source (upper right).

include MS0735.6+7421 [66] which is shown in Fig. 6, Hydra A [67], and Herc A [68].

For the majority of the bubbles which are expanding subsonically or mildly transonically, the pressure within the bubbles must be comparable to the pressure in the X-ray gas external to the bubbles. For the sources with supersonic expansion, the internal pressures must be even higher. However, when the pressures in the radio lobes are estimated by the standard minimum energy or equipartition arguments, they are found to be ~ 20 times smaller than required in most cases (e.g., [54]). This indicates that we have not identified the primary energy content and pressure source within radio sources. It may be that the magnetic fields are larger than given by equipartition. The extra pressure might be due to a large population of low energy relativistic electrons, or to a very large population of relativistic ions. Alternatively, the radio sources may contain diffuse but very hot thermal gas, which provides most of the energy and pressure. Within the radio sources, jet kinetic energy is dissipated by shocks or other friction processes, so it would not be surprising if most of the energy was thermalized. So far, it has been difficult to detect such hot gas in X-ray spectra of the radio lobes (e.g., [54]). However, it could be detectable with high spatial resolution SZ images [69] or hard X-ray images [e.g., 70].

Although the radio bubbles generally show an anticorrelation between radio and X-ray emission, in a few systems there is evidence for a form of positive correlation. Specifically, columns of cool, dense gas are seen going from the center of the central galaxy out to the radio lobes. Examples include Virgo/M87 [72] and Abell 133 [71] (Fig. 7). One suggestion is that these X-ray features are due to cooler gas from the

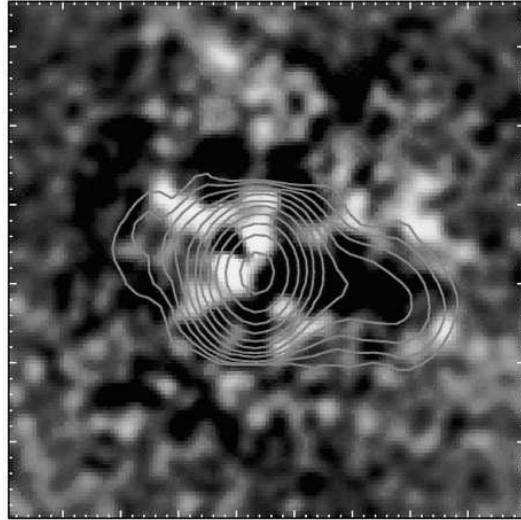


Fig. 8 Greyscale is the Chandra residual image of Abell 2597 after subtraction of an elliptical model, with low frequency (330 MHz) radio contours superposed. The figure is adapted from [74]. The low frequency radio emission extends out into the “ghost bubble” to the west; also, there may be a channel in the X-ray image connecting the ghost bubble with the AGN at the center.

center of the cooling core which has been entrained and uplifted by a buoyant radio lobe.

3.2 Ghost Bubbles in BCGs in Clusters

In many cooling core clusters, “ghost bubbles” are also seen at larger radii from the center. These are holes in the X-ray emission without associated high frequency radio emission. Figure 8 shows Abell 2597, an example of a cooling core with ghost bubbles [73]. Low frequency radio images have detected radio emission in many of the ghost bubbles (e.g., [74]). In general, the properties of the ghost bubbles are consistent with older radio bubbles which have risen buoyantly in the cluster atmosphere. Some examples of ghost bubbles are seen in Perseus [61], Abell 2597 [74], and Abell 262 [75].

3.3 Radio Bubbles in Individual Ellipticals and Groups

Similar radio bubbles and ghost bubbles are seen associated with radio AGNs hosted by ellipticals in groups and individual elliptical galaxies. The Chandra X-ray image

of M84 shows a series of X-ray shells, some of which correspond to components of the radio source [76]. X-ray arcs which may be the sides of radio bubbles are also seen in NGC 4636 [77, 78, 79, 80]. Small bubbles are seen in NGC 4472 [36, 37]. Several groups have small radio bubbles, including NGC 5044 [81], NGC 5098 [82], and HCG 62 [83, 84]. Some of the bubbles in ellipticals appear to be open at their outer edges; this may indicate that the radio sources have blown out the elliptical galaxy gas.

There are a number of surveys of the X-ray emission and radio bubbles in individual elliptical galaxies [e.g., 59, 85, 86, 87, 88, 89]. The Jones et al. [87] sample consisted of 160 nearby gEs, of which 109 had significant X-ray emission from hot gas. The Chandra images of 27 of these ellipticals show evidence for radio bubbles, suggesting that $\gtrsim 25\%$ of early-type galaxies with hot gas have radio bubbles. It is difficult to compare this fraction to that for BCGs in rich clusters due to possible differences in the detectability of bubbles in clusters and gEs. However, the galaxy rate might be similar to the fraction of all clusters which have bubbles, although the fraction of cool core clusters with observed bubbles is higher. A recent radio survey of X-ray-bright ellipticals and S0 found a higher fraction with evidence for radio/X-ray interactions [89].

Surveys of groups find results which are similar to and intermediate between those for clusters and individual galaxies [e.g., 90].

3.4 X-ray Shells as Radio Source Calorimeters

Radio bubbles are very useful systems for determining the total energies supplied by the jets in the radio sources. For the systems which are expanding subsonically, the total energy is the “PdV” work done to displace the X-ray emitting gas, plus the internal energy in the radio bubble [91]. (For systems with shocks, the shock energy needs to be included [66].) This gives a total energy of

$$E_{\text{radio}} = PV + \frac{PV}{\gamma - 1} = \frac{\gamma}{\gamma - 1} PV = (2.5 - 4) PV, \quad (7)$$

where P is the pressure in the radio lobe, V is its volume, and γ is the mean adiabatic index of the contents of the radio lobe. The two terms in the left end of the equation are the work done by the bubble and its internal energy. The range of values at the right of the equation correspond to the range from non-relativistic gas ($\gamma = 5/3$) to relativistic material ($\gamma = 4/3$). For example, in Abell 2052 (Fig. 5), the total energy is $E_{\text{radio}} \approx 10^{59}$ ergs [54], which is a typical value. Similar measurements have provided the best direct evidence on the total energy content of radio jets.

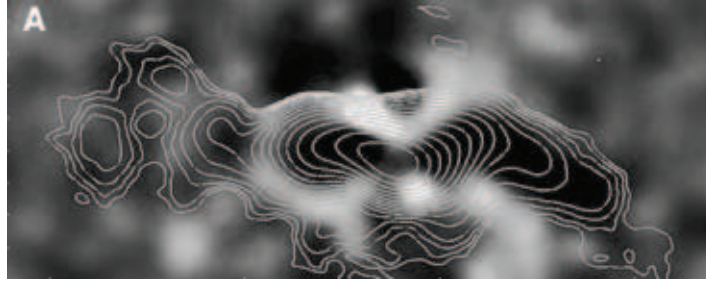


Fig. 9 Residual Chandra X-ray image (greyscale) of the center of Abell 262, showing X-ray cavities to the east and a continuous cavity (“X-ray tunnel”) to the west. The contours are the GMRT 610 MHz radio image, tapered to show the low surface brightness features. This figure was adapted from [75]. The X-ray cavities and radio source are three times longer than seen in previous shallower images, and the total radio source energy is roughly 10 times higher.

3.5 Can Radio Sources Offset Cooling in Cluster Cores?

The energy in the radio source can be compared to the cooling X-ray luminosity of the cooling core to see if it is energetically possible for the radio source to inhibit the radiative cooling of the gas. To make this comparison, one needs a time scale for the activity of the radio source; typically, this is given by the buoyancy rise time of the radio bubbles. Then, the total energy injected by the radio source can be divided by the time scale for the activity to give the power injected by the radio source.

A number of surveys have compared the energy injected by the radio sources with the X-ray luminosity of the cool core region of the cluster where the radiative cooling time is short [92, 93, 94, 95]. In most cases, this comparison indicates that energy from the radio source could balance radiative cooling (e.g., [92]), although this is not true in all cases. Radio heating (as well as the common occurrence of radio sources in cooling cores) requires that the radio activity be episodic; it may be that the average radio power is more important than the current value.

Also, as deeper low frequency radio observations and deeper X-ray observations have been made of clusters, the sizes of the radio bubbles and their total energies are often found to increase. Fig. 9 shows an example, the cluster Abell 262. Previous shallower radio and Chandra X-ray images [96] indicated that the radio sources was roughly 10 times too weak to offset cooling at the center of this cluster. However, a longer Chandra image revealed a long “X-ray tunnel” to the west, and a shorter tunnel plus three additional bubbles to the east. Sensitive low frequency radio observations with the VLA and GMRT have shown that the radio source extends more than three times further than was seen before. The estimate of the total energy of the radio source was increased by roughly 10 times, and now agrees with the cooling luminosity within the errors.

3.6 Can Radio Source Heating Offset Cooling in Individual Ellipticals?

Similar comparisons of the radio source power and the X-ray cooling luminosity have been made for individual elliptical galaxies [88, 89]. For the most X-ray luminous systems, the X-ray cooling luminosity and radio power are in reasonable agreement. However, for ellipticals with lower X-ray cooling luminosities ($\lesssim 5 \times 10^{41}$ erg s⁻¹), the radio power estimated from the radio bubbles significantly exceeds the cooling X-ray luminosity. For these systems, the radio source could heat up and expel the cooling X-ray gas.

3.7 Radiative Efficiency of Radio Jets

Radio bubbles allow the estimation of the total amount of kinetic energy deposited by radio jets, and the power or rate at which this energy is deposited. These values can be compared to the radio luminosity of the jets to determine the efficiency of synchrotron emission. These results show that radio jets are generally quite inefficient; the typical value is $\sim 1\%$ [97]. The efficiency is also highly variable from radio galaxy to galaxy, with a spread of $\sim 10^2$.

3.8 Bondi Accretion vs. Jet Power

Ultimately, the source of the energy in radio jets is thought to be accretion by the SMBH. One can compare the rate of kinetic energy or jet power estimated from the radio bubbles with possible rates of accretion by the SMBH. Perhaps the simplest mode of accretion would be the direct accretion of hot gas from the surrounding elliptical galaxy and/or cluster cool core. Assuming a spherically symmetric system and no angular momentum, the rate of this accretion should be given approximately by the Bondi [98] accretion formula,

$$\dot{M}_{\text{Bondi}} = \frac{\pi}{4} c_s \rho_A r_A^2, \quad (8)$$

where r_A is the accretion radius, c_s is the sound speed in the gas at the accretion radius, and ρ_A is the gas density at the accretion radius. The numerical coefficient in Eq. 8 assumes that the adiabatic index γ of the gas is 5/3. Assuming the SMBH dominates the gravity in the region of interest, the accretion radius is given by

$$r_A = \frac{2GM_{\text{BH}}}{c_s^2}, \quad (9)$$

where M_{BH} is the mass of the BH. In some nearby elliptical galaxies, this radius is comparable to the resolution of Chandra, so that one could determine the gas properties at the accretion radius directly.

Allen et al. [99] compared the Bondi accretion rates for nearby ellipticals with the total power in the jets as determined from their radio bubbles. They found that they correlated, and that the jet powers could be produced if $\sim 2\%$ of the rest mass of the material entering the accretion radius was converted in jet kinetic energy by the black hole.

On the other hand, Rafferty et al. found that Bondi accretion might not work for the most luminous systems, which were generally associated with BCGs. One caveat is that these systems are usually further away, so that the Bondi accretion radius was not resolved in the X-ray observations.

3.9 The Need for Feedback Coupling AGN and X-ray Cooling

In general, AGNs have a very large range in their luminosities, which presumably reflects, at least in part, a large range in their energy output. Thus, it would seem unlikely that heating by radio sources would balance radiative cooling by X-ray gas in cluster cool core in every case without some sort of “feedback” between the AGN activity and the cooling of the gas. If the AGN is powered by the accretion of cooled X-ray gas, such a feedback loop seems possible. For example, consider a cluster containing a BCG with a supermassive black hole at its center. Assume the cluster formed recently or underwent a major merger, and that there is initially no gas which has cooled at the center of the cluster. Thus, the cluster would lack a cool core, and the AGN would be inactive due to a lack of material to accrete. Eventually, radiative cooling would lead some gas to cool at the center of the cluster where the density is highest, and thus the cooling time is shortest. This would lead to gas cooling at the center of the cluster, and some small fraction of this gas would reach the central supermassive black hole and be accreted. The AGN would become active, and would launch jets into the surrounding cluster cool core. Assume that these jets are stopped in the cool core and heat the gas there, suppressing cooling. This would stop the cooling, and eventually starve the AGN of fuel. This might either lead to a stable balance in which just enough gas cooled to low temperatures to power the AGN sufficiently to heat the cool core gas enough to prevent further cooling. Perhaps more likely, this would lead to an episodic limit cycle, with periods of cooling and AGN activity, and the average heating rate by the AGN nearly balancing the average cooling rate by the X-ray gas.

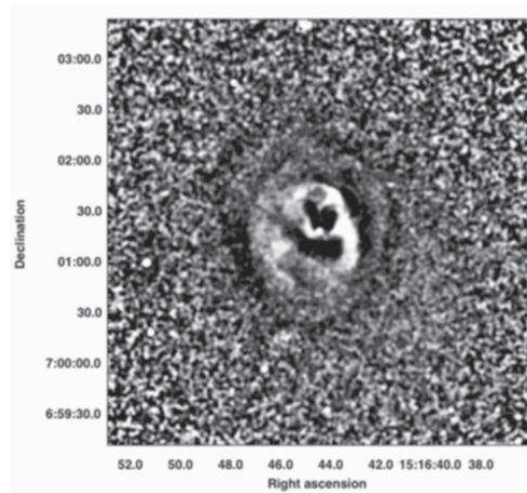


Fig. 10 Unsharp-masked Chandra X-ray image of the center of Abell 2052, showing the radio bubbles and a series of ripples. (The result of a shallower Chandra image is shown in Fig. 5.) The ripples are consistent with sound waves or weak shocks. This figure was adapted from [100].

3.10 Radio Source Heating Mechanism in Cool Cores

Although the radio sources in the centers of cluster cool cores have enough energy, in most cases, to suppress cooling (Sects. 3.5 & 3.6), the detailed mechanism by which they heat the gas is still poorly understood. How can one get heat preferentially into the cooler gas? How is the heat transported to the outer parts of the cool core without disrupting (e.g., by convection) the cool core and the observed abundance gradients there? It may be that the radio plasma mixes with the X-ray plasma, or that relativistic particles diffuse into the thermal gas, and directly heat the gas. Heat conduction may carry energy from hot gas into cooler gas. The buoyant rise of the bubbles will release gravitational energy and heat the gas. The X-ray gas might be heated by plasma waves, sound waves, or weak shocks generated by the radio source. The deep Chandra image of the center of the Perseus cluster shows ripples which are probably sound waves and weak shocks from the radio source [61]. Fig. 10 shows an unsharp-masked Chandra image of the center of Abell 2052, which shows similar ripples [100].

The problem of heating is complicated by the fact that the energy is initially in the directed flow of the radio jets. How do initially narrow radio jets heat the X-ray gas in all directions (e.g., [101])? Sound waves and shocks might be useful for isotropizing the heating. Why don't the jets just punch narrow channels in the gas? Is the collimated outflow disrupted by jet precession, or cluster gas motions, or instabilities? Does most of the energy actually come out in wider jets or winds? The

detailed nature of the AGN heating and feedback in cool cores is a very active area of research.

3.11 The Southwest Radio Lobe of Cen-A

Centaurus A (Cen A or NGC 5128) is the nearest bright elliptical galaxy, the nearest radio galaxy, and possibly the nearest powerful AGN. This makes it an ideal candidate for the detail study of the interaction between radio sources and the hot gas in ellipticals. Recently, Cen A was observed for roughly 740 ksec with Chandra as part of a Very Large Program (Ralph Kraft PI). Part of this project involved a detailed study of the southwest radio lobe by Croston et al. [102]. Fig. 11 shows the X-ray and radio images of this region. The SW radio lobe is surrounded by a thin shell of X-ray emission which has a very sharp outer boundary. There is very little diffuse emission from beyond this shell. Based on earlier observations, it had been suggested that this X-ray shell was thermal emission from hot interstellar gas shocked by the expansion of the radio lobe [103]. This would make the SW lobe in Cen A similar to the radio bubbles discussed above, but with a much higher Mach number for the expansion. One problem with this suggestion is that the compression required to explain the large increase in X-ray surface brightness at the outer edge of the X-ray shell is much greater than four, the highest value possible for a non-cooling shock.

The new observations from the Very Large Program show that the emission from this shell is actually nonthermal rather than thermal [102]. Apparently, the gas density in this region is so low that the thermal emission from the shock driven by the expanding radio lobe is too small to detect. The observed X-ray emission is probably X-ray synchrotron emission. Thus, this lobe is similar to the nonthermal supernova remnant shocks, such as in SNR1006. The observations indicate that the lobe is expanding at $\sim 2600 \text{ km s}^{-1}$, which corresponds to a Mach number of ~ 8 . It is likely that electrons are being accelerated up to energies of $\sim 10^{14}$ eV. These observations suggest that the SW lobe should be a detectable source of TeV gamma-rays, but that it is probably not the source of the Ultra-High Energy Cosmic Rays which come from the direction of Cen A.

Acknowledgements I thank Liz Blanton, Tracy Clarke, Judith Croston, and Ming Sun for comments and help with the figures for the original talk which led to this chapter. I want to thank Dong-Woo Kim and Silvia Pellegrini for organizing the very useful Joint Discussion at the IAU General Assembly in Rio, and for editing this volume. This work was supported by NASA Chandra grants GO7-8078X, GO7-8081A, GO8-9083X, GO8-9085X, GO9-0135X, and GO9-0148X, and NASA Herschel grant RSA1373266, and NASA HST grants HST-GO-10597.03-A and HST-GO-11679.01.

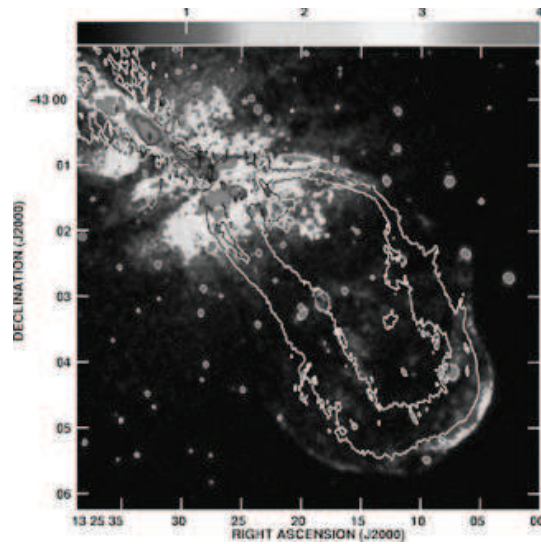


Fig. 11 The SW radio lobe of Cen A. The grey scale shows the Chandra X-ray image, while the contours are from the 1.4 GHz radio image. This figure was adapted from [102, Fig. 1]. Note that the radio lobe is surrounded by a thin shell of X-ray emission, and that the thin shell has a very sharp outer boundary with little emission beyond the shell.

References

- [1] R.E. White, III, C.L. Sarazin, *ApJ* **367**, 476 (1991). DOI 10.1086/169644
- [2] M. Henriksen, S. Cousineau, *ApJ* **511**, 595 (1999). DOI 10.1086/306690
- [3] T.E. Jeltema, B. Binder, J.S. Mulchaey, *ApJ* **679**, 1162 (2008). DOI 10.1086/587508
- [4] A. Finoguenov, U.G. Briel, J.P. Henry, G. Gavazzi, J. Iglesias-Paramo, A. Boselli, *A&Ap* **419**, 47 (2004). DOI 10.1051/0004-6361:20035765
- [5] A.E. Hornschemeier, B. Mobasher, D.M. Alexander, F.E. Bauer, M.W. Bautz, D. Hammer, B.M. Poggianti, *ApJ* **643**, 144 (2006). DOI 10.1086/500798
- [6] R.J. Smith, *MNRAS* **344**, L17 (2003). DOI 10.1046/j.1365-8711.2003.06963.x
- [7] M. Sun, C. Jones, W. Forman, A. Vikhlinin, M. Donahue, M. Voit, *ApJ* **657**, 197 (2007). DOI 10.1086/510895
- [8] B.A. Brown, J.N. Bregman, *ApJ* **539**, 592 (2000). DOI 10.1086/309240
- [9] E. O’Sullivan, D.A. Forbes, T.J. Ponman, *MNRAS* **328**, 461 (2001). DOI 10.1046/j.1365-8711.2001.04890.x
- [10] S.F. Helsdon, T.J. Ponman, E. O’Sullivan, D.A. Forbes, *MNRAS* **325**, 693 (2001). DOI 10.1046/j.1365-8711.2001.04490.x
- [11] S.C. Ellis, E. O’Sullivan, *MNRAS* **367**, 627 (2006). DOI 10.1111/j.1365-2966.2005.09982.x

- [12] J.S. Mulchaey, T.E. Jeltema, *ApJ* **715**, L1 (2010). DOI 10.1088/2041-8205/715/1/L1
- [13] E. Memola, G. Trinchieri, A. Wolter, P. Focardi, B. Kelm, *A&Ap* **497**, 359 (2009). DOI 10.1051/0004-6361/200810801
- [14] S. Diehl, T.S. Statler, *ApJ* **687**, 986 (2008). DOI 10.1086/592179
- [15] J.E. Gunn, J.R. Gott, III, *ApJ* **176**, 1 (1972). DOI 10.1086/151605
- [16] C.L. Sarazin, *ApL***20**, 93 (1979)
- [17] I.G. McCarthy, C.S. Frenk, A.S. Font, C.G. Lacey, R.G. Bower, N.L. Mitchell, M.L. Balogh, T. Theuns, *MNRAS* **383**, 593 (2008). DOI 10.1111/j.1365-2966.2007.12577.x
- [18] D.M. Acreman, I.R. Stevens, T.J. Ponman, I. Sakelliou, *MNRAS* **341**, 1333 (2003). DOI 10.1046/j.1365-8711.2003.06504.x
- [19] V. Quilis, B. Moore, R. Bower, *Science* **288**, 1617 (2000). DOI 10.1126/science.288.5471.1617
- [20] E. Roediger, M. Brüggen, *MNRAS* **388**, L89 (2008). DOI 10.1111/j.1745-3933.2008.00506.x
- [21] P.E.J. Nulsen, *MNRAS* **198**, 1007 (1982)
- [22] L.J. Spitzer, *Physics of Fully Ionized Gases* (Interscience, New York, 1956)
- [23] L.L. Cowie, A. Songaila, *Nat***266**, 501 (1977). DOI 10.1038/266501a0
- [24] M. Brüggen, G. De Lucia, *MNRAS* **383**, 1336 (2008). DOI 10.1111/j.1365-2966.2007.12670.x
- [25] W. Domainko, M. Mair, W. Kapferer, E. van Kampen, T. Kronberger, S. Schindler, S. Kimeswenger, M. Ruffert, O.E. Mangete, *A&Ap* **452**, 795 (2006). DOI 10.1051/0004-6361:20053921
- [26] A. Vikhlinin, M. Markevitch, S.S. Murray, *ApJ* **551**, 160 (2001)
- [27] M. Markevitch, T.J. Ponman, P.E.J. Nulsen, M.W. Bautz, D.J. Burke, L.P. David, D. Davis, R.H. Donnelly, W.R. Forman, C. Jones, J. Kaastra, E. Kellogg, D.W. Kim, J. Kolodziejczak, P. Mazzotta, A. Pagliaro, S. Patel, L. Van Speybroeck, A. Vikhlinin, J. Vrtilik, M. Wise, P. Zhao, *ApJ* **541**, 542 (2000)
- [28] M. Markevitch, A. Vikhlinin, *PhysRep***443**, 1 (2007). DOI 10.1016/j.physrep.2007.01.001
- [29] L.D. Landau, E.M. Lifshitz, *Fluid Mechanics* (Pergamon, Oxford, 1959)
- [30] C.L. Sarazin, in *Merging Processes in Galaxy Clusters*, ed. by L. Feretti, I.M. Gioia, G. Giovannini (Kluwer, Dordrecht, 2002), pp. 1–38
- [31] S. Schreier, *Compressible Flow* (Wiley, New York, 1982), pp. 182–189
- [32] J.A. Irwin, C.L. Sarazin, *ApJ* **471**, 683 (1996). DOI 10.1086/177998
- [33] W. Forman, J. Schwarz, C. Jones, W. Liller, A.C. Fabian, *ApJ* **234**, L27 (1979). DOI 10.1086/183103
- [34] F.V.N. Rangarajan, D.A. White, H. Ebeling, A.C. Fabian, *MNRAS* **277**, 1047 (1995)
- [35] S. Randall, P. Nulsen, W.R. Forman, C. Jones, M. Machacek, S.S. Murray, B. Maughan, *ApJ* **688**, 208 (2008). DOI 10.1086/592324
- [36] B.A. Biller, C. Jones, W.R. Forman, R. Kraft, T. Ensslin, *ApJ* **613**, 238 (2004). DOI 10.1086/423020

- [37] R. Kraft, W.R. Forman, C. Jones, P.E.J. Nulsen, M.J. Hardcastle, S. Raychaudhury, D.A. Evans, G. Sivakoff, C. Sarazin, *ApJ* p. submitted (2010)
- [38] M. Machacek, C. Jones, W.R. Forman, P. Nulsen, *ApJ* **644**, 155 (2006). DOI 10.1086/503350
- [39] G. Trinchieri, G. Fabbiano, D. Kim, *A&Ap* **318**, 361 (1997)
- [40] D. Kim, E. Kim, G. Fabbiano, G. Trinchieri, *ApJ* **688**, 931 (2008). DOI 10.1086/592211
- [41] S.W. Randall, C. Jones, R. Kraft, W.R. Forman, E. O'Sullivan, *ApJ* **696**, 1431 (2009). DOI 10.1088/0004-637X/696/2/1431
- [42] M. Machacek, A. Dosaj, W. Forman, C. Jones, M. Markevitch, A. Vikhlinin, A. Warmflash, R. Kraft, *ApJ* **621**, 663 (2005). DOI 10.1086/427548
- [43] C.A. Scharf, D.R. Zurek, M. Bureau, *ApJ* **633**, 154 (2005). DOI 10.1086/444531
- [44] M. Sun, D. Jerius, C. Jones, *ApJ* **633**, 165 (2005). DOI 10.1086/452620
- [45] G.R. Sivakoff, C.L. Sarazin, J.L. Carlin, *ApJ* **617**, 262 (2004). DOI 10.1086/425244
- [46] M.E. Machacek, R.P. Kraft, C. Jones, W.R. Forman, M.J. Hardcastle, *ApJ* **664**, 804 (2007). DOI 10.1086/519233
- [47] I. Sakelliou, M.R. Merrifield, I.M. McHardy, *MNRAS* **283**, 673 (1996)
- [48] Q.D. Wang, F. Owen, M. Ledlow, W. Keel, in *IAU Colloq. 195: Outskirts of Galaxy Clusters: Intense Life in the Suburbs*, ed. by A. Diaferio (2004), pp. 78–82. DOI 10.1017/S174392130400016X
- [49] A. Vikhlinin, M. Markevitch, W. Forman, C. Jones, *ApJ* **555**, L87 (2001). DOI 10.1086/323181
- [50] N.Y. Yamasaki, T. Ohashi, T. Furusho, *ApJ* **578**, 833 (2002). DOI 10.1086/342652
- [51] M. Sun, A. Vikhlinin, W. Forman, C. Jones, S.S. Murray, *ApJ* **619**, 169 (2005). DOI 10.1086/425298
- [52] M. Sun, *ApJ* **704**, 1586 (2009). DOI 10.1088/0004-637X/704/2/1586
- [53] E.L. Blanton, C.L. Sarazin, B.R. McNamara, M.W. Wise, *ApJ* **558**, L15 (2001). DOI 10.1086/323269
- [54] E.L. Blanton, C.L. Sarazin, B.R. McNamara, *ApJ* **585**, 227 (2003). DOI 10.1086/345984
- [55] J. Magorrian, S. Tremaine, D. Richstone, R. Bender, G. Bower, A. Dressler, S.M. Faber, K. Gebhardt, R. Green, C. Grillmair, J. Kormendy, T. Lauer, *AJ* **115**, 2285 (1998). DOI 10.1086/300353
- [56] S. Tremaine, K. Gebhardt, R. Bender, G. Bower, A. Dressler, S.M. Faber, A.V. Filippenko, R. Green, C. Grillmair, L.C. Ho, J. Kormendy, T.R. Lauer, J. Magorrian, J. Pinkney, D. Richstone, *ApJ* **574**, 740 (2002). DOI 10.1086/341002
- [57] D.J. Croton, V. Springel, S.D.M. White, G. De Lucia, C.S. Frenk, L. Gao, A. Jenkins, G. Kauffmann, J.F. Navarro, N. Yoshida, *MNRAS* **365**, 11 (2006). DOI 10.1111/j.1365-2966.2005.09675.x
- [58] J.R. Peterson, A.C. Fabian, *PhysRep* **427**, 1 (2006). DOI 10.1016/j.physrep.2005.12.007

- [59] B.R. McNamara, P.E.J. Nulsen, *ARAA***45**, 117 (2007). DOI 10.1146/annurev.astro.45.051806.110625
- [60] D.S. Hudson, R. Mittal, T.H. Reiprich, P.E.J. Nulsen, H. Andernach, C.L. Sarazin, *A&Ap* **513**, A37+ (2010). DOI 10.1051/0004-6361/200912377
- [61] A.C. Fabian, J.S. Sanders, G.B. Taylor, S.W. Allen, C.S. Crawford, R.M. Johnstone, K. Iwasawa, *MNRAS* **366**, 417 (2006). DOI 10.1111/j.1365-2966.2005.09896.x
- [62] C.L. Sarazin, R.W. O'Connell, B.R. McNamara, *ApJ* **389**, L59 (1992). DOI 10.1086/186348
- [63] H. Böhringer, W. Voges, A.C. Fabian, A.C. Edge, D.M. Neumann, *MNRAS* **264**, L25 (1993)
- [64] Z. Huang, C.L. Sarazin, *ApJ* **496**, 728 (1998). DOI 10.1086/305406
- [65] E. Rizza, C. Loken, M. Bliton, K. Roettiger, J.O. Burns, F.N. Owen, *AJ* **119**, 21 (2000). DOI 10.1086/301167
- [66] B.R. McNamara, P.E.J. Nulsen, M.W. Wise, D.A. Rafferty, C. Carilli, C.L. Sarazin, E.L. Blanton, *Nat***433**, 45 (2005). DOI 10.1038/nature03202
- [67] P.E.J. Nulsen, B.R. McNamara, M.W. Wise, L.P. David, *ApJ* **628**, 629 (2005). DOI 10.1086/430845
- [68] P.E.J. Nulsen, D.C. Hambrick, B.R. McNamara, D. Rafferty, L. Birzan, M.W. Wise, L.P. David, *ApJ* **625**, L9 (2005). DOI 10.1086/430945
- [69] C. Pfammer, T.A. Enßlin, C.L. Sarazin, *A&Ap* **430**, 799 (2005). DOI 10.1051/0004-6361:20041576
- [70] J.E. Koglin, H. An, K.L. Blaedel, N.F. Brejnholt, F.E. Christensen, W.W. Craig, T.A. Decker, C.J. Hailey, L.C. Hale, F.A. Harrison, C.P. Jensen, K.K. Madsen, K. Mori, M.J. Pivovarov, G. Tajiri, W.W. Zhang, in *Society of Photo-Optical Instrumentation Engineers (SPIE) Conference Series, Society of Photo-Optical Instrumentation Engineers (SPIE) Conference Series*, vol. 7437 (2009), *Society of Photo-Optical Instrumentation Engineers (SPIE) Conference Series*, vol. 7437. DOI 10.1117/12.826724
- [71] Y. Fujita, C.L. Sarazin, J.C. Kempner, L. Rudnick, O.B. Slee, A.L. Roy, H. Andernach, M. Ehle, *ApJ* **575**, 764 (2002). DOI 10.1086/341352
- [72] A.J. Young, A.S. Wilson, C.G. Mundell, *ApJ* **579**, 560 (2002). DOI 10.1086/342918
- [73] B.R. McNamara, M.W. Wise, P.E.J. Nulsen, L.P. David, C.L. Carilli, C.L. Sarazin, C.P. O'Dea, J. Houck, M. Donahue, S. Baum, M. Voit, R.W. O'Connell, A. Koekemoer, *ApJ* **562**, L149 (2001). DOI 10.1086/338326
- [74] T.E. Clarke, C.L. Sarazin, E.L. Blanton, D.M. Neumann, N.E. Kassim, *ApJ* **625**, 748 (2005). DOI 10.1086/429717
- [75] T.E. Clarke, E.L. Blanton, C.L. Sarazin, L.D. Anderson, Gopal-Krishna, E.M. Douglass, N.E. Kassim, *ApJ* **697**, 1481 (2009). DOI 10.1088/0004-637X/697/2/1481
- [76] A. Finoguenov, M. Ruszkowski, C. Jones, M. Brügggen, A. Vikhlinin, E. Mandel, *ApJ* **686**, 911 (2008). DOI 10.1086/591662
- [77] C. Jones, W. Forman, A. Vikhlinin, M. Markevitch, L. David, A. Warmflash, S. Murray, P.E.J. Nulsen, *ApJ* **567**, L115 (2002). DOI 10.1086/340114

- [78] A. Ohto, N. Kawano, Y. Fukazawa, PASJ **55**, 819 (2003)
- [79] E. O’Sullivan, J.M. Vrtilek, J.C. Kempner, ApJ **624**, L77 (2005). DOI 10.1086/430600
- [80] A. Baldi, W. Forman, C. Jones, R. Kraft, P. Nulsen, E. Churazov, L. David, S. Giacintucci, ApJ **707**, 1034 (2009). DOI 10.1088/0004-637X/707/2/1034
- [81] L.P. David, C. Jones, W. Forman, P. Nulsen, J. Vrtilek, E. O’Sullivan, S. Giacintucci, S. Raychaudhury, ApJ **705**, 624 (2009). DOI 10.1088/0004-637X/705/1/624
- [82] S.W. Randall, C. Jones, M. Markevitch, E.L. Blanton, P.E.J. Nulsen, W.R. Forman, ApJ **700**, 1404 (2009). DOI 10.1088/0004-637X/700/2/1404
- [83] U. Morita, Y. Ishisaki, N.Y. Yamasaki, N. Ota, N. Kawano, Y. Fukazawa, T. Ohashi, PASJ **58**, 719 (2006)
- [84] M. Gitti, E. O’Sullivan, S. Giacintucci, L.P. David, J. Vrtilek, S. Raychaudhury, P.E.J. Nulsen, ApJ **714**, 758 (2010). DOI 10.1088/0004-637X/714/1/758
- [85] W.G. Mathews, F. Brighenti, ARAA**41**, 191 (2003). DOI 10.1146/annurev.astro.41.090401.094542
- [86] S. Diehl, T.S. Statler, ApJ **680**, 897 (2008). DOI 10.1086/587481
- [87] C. Jones, W. Forman, E. Churazov, P. Nulsen, R. Kraft, S. Murray, in *Heating versus Cooling in Galaxies and Clusters of Galaxies*, ed. by H. Böhringer, G. W. Pratt, A. Finoguenov, & P. Schuecker (2007), pp. 145–+
- [88] P.E.J. Nulsen, C. Jones, W.R. Forman, L.P. David, B.R. McNamara, D.A. Rafferty, L. Bîrzan, M.W. Wise, in *Heating versus Cooling in Galaxies and Clusters of Galaxies*, ed. by H. Böhringer, G. W. Pratt, A. Finoguenov, & P. Schuecker (2007), pp. 210–+
- [89] R.J.H. Dunn, S.W. Allen, G.B. Taylor, K.F. Shurkin, G. Gentile, A.C. Fabian, C.S. Reynolds, MNRAS **404**, 180 (2010). DOI 10.1111/j.1365-2966.2010.16314.x
- [90] R. Dong, J. Rasmussen, J.S. Mulchaey, ApJ **712**, 883 (2010). DOI 10.1088/0004-637X/712/2/883
- [91] E. Churazov, R. Sunyaev, W. Forman, H. Böhringer, MNRAS **332**, 729 (2002). DOI 10.1046/j.1365-8711.2002.05332.x
- [92] L. Bîrzan, D.A. Rafferty, B.R. McNamara, M.W. Wise, P.E.J. Nulsen, ApJ **607**, 800 (2004). DOI 10.1086/383519
- [93] R.J.H. Dunn, A.C. Fabian, MNRAS **373**, 959 (2006). DOI 10.1111/j.1365-2966.2006.11080.x
- [94] D.A. Rafferty, B.R. McNamara, P.E.J. Nulsen, M.W. Wise, ApJ **652**, 216 (2006). DOI 10.1086/507672
- [95] R.J.H. Dunn, A.C. Fabian, MNRAS **385**, 757 (2008). DOI 10.1111/j.1365-2966.2008.12898.x
- [96] E.L. Blanton, C.L. Sarazin, B.R. McNamara, T.E. Clarke, ApJ **612**, 817 (2004). DOI 10.1086/422677
- [97] L. Bîrzan, B.R. McNamara, P.E.J. Nulsen, C.L. Carilli, M.W. Wise, ApJ **686**, 859 (2008). DOI 10.1086/591416
- [98] H. Bondi, MNRAS **112**, 195 (1952)

- [99] S.W. Allen, R.J.H. Dunn, A.C. Fabian, G.B. Taylor, C.S. Reynolds, *MNRAS* **372**, 21 (2006). DOI 10.1111/j.1365-2966.2006.10778.x
- [100] E.L. Blanton, S.W. Randall, E.M. Douglass, C.L. Sarazin, T.E. Clarke, B.R. McNamara, *ApJ* **697**, L95 (2009). DOI 10.1088/0004-637X/697/2/L95
- [101] J.C. Vernaleo, C.S. Reynolds, *ApJ* **645**, 83 (2006). DOI 10.1086/504029
- [102] J.H. Croston, R.P. Kraft, M.J. Hardcastle, M. Birkinshaw, D.M. Worrall, P.E.J. Nulsen, R.F. Penna, G.R. Sivakoff, A. Jordán, N.J. Brassington, D.A. Evans, W.R. Forman, M. Gilfanov, J.L. Goodger, W.E. Harris, C. Jones, A.M. Juett, S.S. Murray, S. Raychaudhury, C.L. Sarazin, R. Voss, K.A. Woodley, *MNRAS* **395**, 1999 (2009). DOI 10.1111/j.1365-2966.2009.14715.x
- [103] R.P. Kraft, S.E. Vázquez, W.R. Forman, C. Jones, S.S. Murray, M.J. Hardcastle, D.M. Worrall, E. Churazov, *ApJ* **592**, 129 (2003). DOI 10.1086/375533